Vision Research 205 (2023) 108174

Contents lists available at ScienceDirect

Vision Research

journal homepage: www.elsevier.com/locate/visres

Tilt aftereffect spreads across the visual field

Busra Tugce Gurbuz [a,*], Huseyin Boyaci [a,b,c,*]

[a] Aysel Sabuncu Brain Research Center & National Magnetic Resonance Research Center (UMRAM), Bilkent University, Ankara, Turkey
[b] Department of Psychology, Bilkent University, Ankara, Turkey
[c] Department of Psychology, Justus Liebig University Giessen, Giessen, Germany

ARTICLE INFO

Keywords:
Orientation perception
Tilt aftereffect
Receptive field

ABSTRACT

The tilt aftereffect (TAE) is observed when adaptation to a tilted contour alters the perceived tilt of a subsequently presented contour. Thus far, TAE has been treated as a local aftereffect observed only at the location of the adapter. Whether and how TAE spreads to other locations in the visual field has not been systematically studied. Here, we sought an answer to this question by measuring TAE magnitudes at locations including but not limited to the adapter location. The adapter was a tilted grating presented at the same peripheral location throughout an experimental session. In a single trial, participants indicated the perceived tilt of a test grating presented after the adapter at one of fifteen locations in the same visual hemifield as the adapter. We found non-zero TAE magnitudes in all locations tested, showing that the effect spreads across the tested visual hemifield. Next, to establish a link between neuronal activity and behavioral results and to predict the possible neuronal origins of the spread, we built a computational model based on known characteristics of the visual cortex. The simulation results showed that the model could successfully capture the pattern of the behavioral results. Furthermore, the pattern of the optimized receptive field sizes suggests that mid-level visual areas, such as V4, could be critically involved in TAE and its spread across the visual field.

1. Introduction

Perceived orientation of a two-dimensional contour is strongly affected by the observer's state of adaptation. For example, sustained exposure to an oriented contour may change the perceived orientation of a subsequently presented contour, a phenomenon known as the tilt aftereffect (TAE) (Gibson & Radner, 1937). Besides orientation, similar adaptation effects are observed in other stimulus dimensions, such as motion (Anstis, Verstraten, & Mather, 1998), color (McCollough, 1965), and size (Blakemore & Sutton, 1969).

Previous studies have commonly treated TAE as a local effect and investigated the behavioral and neuronal responses with test contours presented at the same location as the adapter. Physiological studies done in this way revealed two main changes in neuronal responses as a result of adaptation: (1) relative fatigue or suppression in response amplitudes of neurons tuned closer to the adapter orientation (Blakemore & Campbell, 1969), and (2) shift in neurons' preference away from the adapter orientation (Dragoi, Sharma, & Sur, 2000) (also see Alink, Abdulrahman, & Henson (2018), Clifford et al. (2001)). These two mechanisms lead to different perceptual outcomes. The former leads to a repulsive shift in the population response and causes a perception away from the adapter orientation. In contrast, the latter leads to a population response attracted toward the adapter and cause a perception closer to the adapter orientation. Models combining the two mechanisms were able to predict TAE more successfully compared to those based on only a single mechanism (Jin, Dragoi, Sur, & Seung, 2005). Accordingly, it was argued that both mechanisms play a role in TAE; the suppression of neuronal responses constitutes the repulsive effect observed in TAE, whereas shifts in neuronal preferences weaken the effect and reduce perceptual errors. Fig. 1 depicts the simultaneous effect of these two mechanisms.

There may be benefits of this type of adaptation aftereffects for the visual system. For instance, it could serve as a gain control mechanism to maximize visual processing efficiency by increasing the saliency of the novel visual input (McDermott, Malkoc, Mulligan, & Webster, 2010). Naturally, one might expect that these benefits would not be tied to the adapter location to allow efficient processing across the visual field. In general, however, TAE and other perceptual aftereffects are commonly

* Corresponding authors at: Department of Quantitative Life Sciences, McGill University, Montréal, Québec, Canada; Montréal Neurological Institute - Hospital, Montréal, Quebec, Canada; Mila - Québec Artificial Intelligence Institute, Montréal, Québec, Canada; CHU Sainte - Justine, Montréal, Québec, Canada. (B. T. Gurbuz) Aysel Sabuncu Brain Research Center & National Magnetic Resonance Research Center (UMRAM), Bilkent University, Ankara, Turkey (H. Boyaci).
E-mail addresses: tugce.gurbuz@mail.mcgill.ca (B.T. Gurbuz), hboyaci@bilkent.edu.tr (H. Boyaci).

https://doi.org/10.1016/j.visres.2022.108174
Received 6 September 2022; Received in revised form 13 December 2022; Accepted 14 December 2022
Available online 9 January 2023

considered localized with few exceptions (see, for example, Altan & Boyaci (2020) for the spread of size adaptation aftereffect across the visual field). Therefore, how the perceived tilt of a contour is affected by an adapter located at another location in the visual field has not been investigated systematically before.

In this study, we investigate how adaptation to a tilted Gabor patch at one location in the visual hemifield impacts the perceived tilt at other locations. For this purpose, we used two main experimental procedures: a selective-adaptation procedure to a peripheral adapter at a fixed location in the visual hemifield and a testing procedure to test the TAE magnitude at fifteen test locations within the same visual hemifield, including the adapter location. We found that TAE is not limited to the adapted location; it spreads across the tested visual hemifield. Next, to establish possible links with the underlying neuronal mechanisms and hypothesize about the visual cortical areas involved in this effect, we developed and tested a computational model using the aforementioned suppression and shift mechanisms of adaptation. Our model successfully captured the pattern in the empirical data, and the optimized receptive field sizes suggest that mid-level visual areas could be involved in the observed spread of TAE.

2. Experiment

2.1. Materials and methods

2.1.1. Participants

19 right-handed participants (8 Female, 11 Male; age range: 19–27, $M = 21.1; SD = 2.1$) with normal or corrected-to-normal vision took part in the experiment. Participants gave their written informed consent before the experiment. Ethical approval for the experiment was obtained from Bilkent University Human Ethics Committee.

2.1.2. Stimuli and apparatus

Stimuli were presented on a 30-inch NEC MultiSync LCD monitor (60 Hz refresh rate and 1920x1200 pixels resolution) in a dark room. A chin-rest was used to stabilize participants' heads.

Two main stimuli were used in the experiment: adapter and test stimuli, both of which were Gabor patches generated in Python (Version 3.7, available at http://www.python.org) using the PsychoPy library (Version 3.0.1.) (Peirce et al., 2019) in a way that would elicit the maximum TAE magnitude based on previous studies in literature (Harris & Calvert, 1989). All patches had a diameter of 3° (2.7° visible stimuli), 1.0 Michelson contrast, and 1.44 c/deg spatial frequency. The adapter patch was always tilted clockwise, with an orientation of 105° (left-handed coordinate system, where 90° is the vertical orientation), whereas two 1-up-1-down adaptive staircases per test location determined the test patch orientation. Each staircase contained 25 trials, and their starting orientations were 80° and 105°. Within each staircase, the orientation of the test patch in a trial was adjusted by the experimental program based on the participant's responses in previous trials. The step size of the adjustment was 2.0° at the beginning of the procedure, and it was reduced to 1.0° after the first reversal of the participant's orientation judgment, and to 0.5° after the second reversal, and was kept at that level until the end of the trials in that staircase (Nishida, Motoyoshi, Andersen, & Shimojo, 2003).

Participants sat 65 cm away from the screen and fixated on a central fixation point. During an experimental session, the stimuli were presented at only one visual hemifield. Left and right visual hemifield tests were counterbalanced across sessions and participants. The adapter patch flickered with a square-wave modulation at 10 Hz to prevent afterimages and was always presented at 10.5° eccentricity to the fixation point. The test patch was presented at one of the fifteen possible test locations, randomly chosen in a trial, in the same visual hemifield, including the adapter location as shown in Fig. 2. Three rows of the test locations were named relative to the adapter as Center (*C*; same row), Down (*D*; 4° lower row), and Up (*U*; 4° upper row). Five columns of the test locations were named relative to the location of the adapter patch as Center (*C*; same column as the adapter), Near1, and Near2 (*N1, N2*; closer to the fixation point than the adapter by 4° and 8°, respectively), and Further1 and Further2 (*F1, F2*; further from the fixation point than the adapter by 4° and 8°, respectively). Consequently, names of the test gratings were formed by combining their row and column names (e.g., C_{N1}; center row, Near1 column). Because of the symmetry, the same test patch names were used for both visual hemifields.

2.1.3. Procedure and Data Analysis

The experimental procedure was adapted from Altan and Boyaci (2020), and the code for the experimental procedure is publicly available (see Data and Code Availability Statement section). Participants started an experimental block by pressing the space bar on a keyboard after reading the experiment instructions on the screen. They first completed a no-adaptation block followed by an adaptation block. Fig. 3 shows the experimental design of both conditions. For the adaptation condition, an experimental trial started with 5000 ms adaptation to

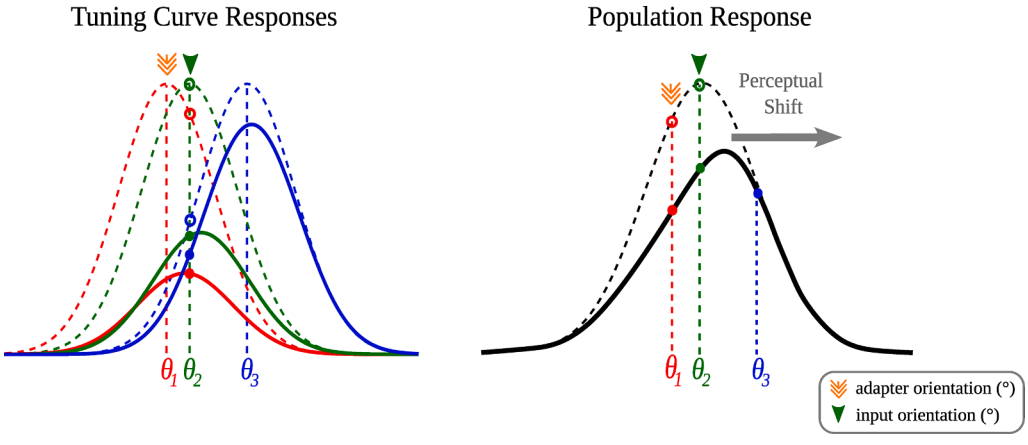

Fig. 1. The suppression and shift models of orientation adaptation. In both panels, the dashed lines represent unadapted neural responses, and the thick lines represent the responses after adaptation. The left panel shows examples of hypothesized responses of neurons with different tuning curves peaking at several orientations (θ_1, θ_2, θ_3). The right panel shows the population responses obtained from the activity of those neurons. Here, we show how the responses change after adapting to an orientation of θ_1. On the left panel, unfilled circles represent the responses of neurons to an orientation of θ_2 before adaptation. The population response obtained with this pattern of activity leads to a peak at θ_2 as shown on the right panel. As a result of adaptation to θ_1, the responses of neurons tuned closer to θ_1 have stronger amplitude suppression than those tuned to further orientations. Moreover, their orientation preference shifts more strongly away from the adapter. The net result of this suppression and shift lead to an overall repulsive shift away from the adapter orientation in the population response. This shift in neural responses can, in principle, predict the perceived shift in orientation and, thus, the tilt aftereffect (TAE). Note that the figure is formed by hypothetical shift and suppression values for demonstration purposes.

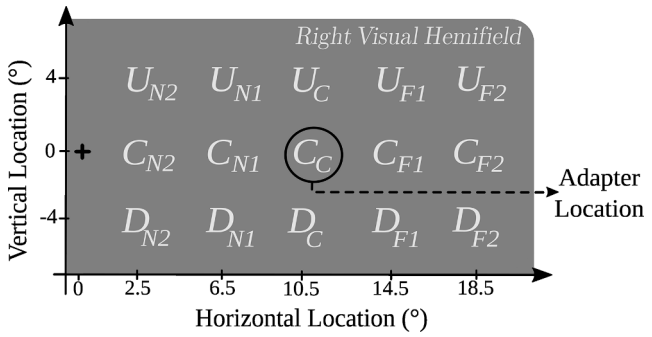

Fig. 2. Naming convention, and locations of the adapter and test patches in the right visual hemifield. The left visual hemifield locations are mirror symmetric of these. The cross is the central fixation point (FP), and the solid circle marks the location of the adapter grating. The first letter of the location names indicates its row relative to the adapter (C: same row; D: 4° lower; U: 4° upper). The subscript refers to the column relative to the adapter (C: same column as the adapter; N1 and N2: nearer to the FP than the adapter by 4° and 8°, respectively; F1 and F2: further from FP than the adapter by 4° and 8°, respectively.).

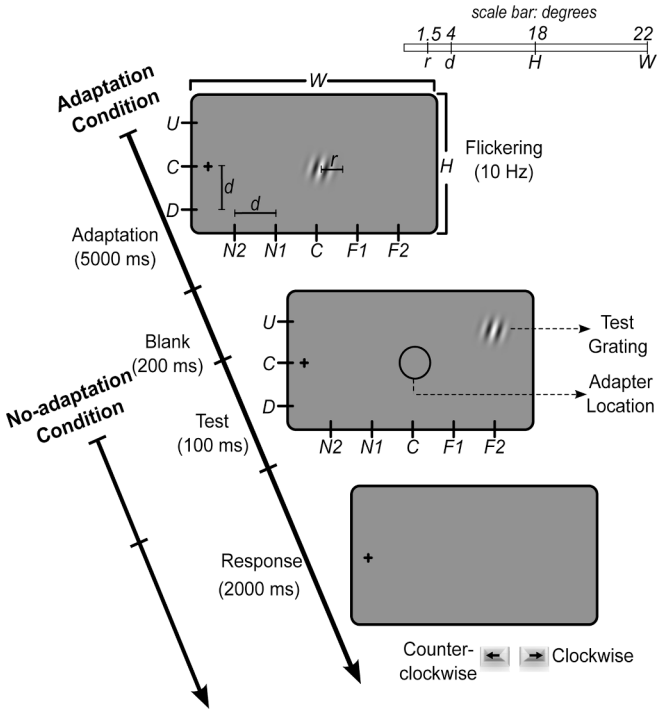

Fig. 3. Experimental design. Adaptation blocks started with a 5000 ms adaptation to a patch that was always presented at the same location (C_C) and tilted clockwise. After a 200 ms blank screen, the test patch was presented at a randomly chosen position among fifteen possible positions (see Fig. 2) for 100 ms. During the following 2000 ms blank screen, participants indicated the perceived tilt of the test patch by pressing the right (i.e., clockwise) or left (i.e., counter-clockwise) arrow key on a keyboard. The no-adaptation condition was identical to the adaptation condition, except for the adaptation phase. The scale bar represents the relative sizes of the screen, adapter grating, and test locations in degrees.

adapter grating, and it was followed by a 200 ms blank screen and 100 ms test grating presentation. Then, a 2000 ms blank screen was presented where participants indicated the perceived tilt of the test grating by pressing the left (for counterclockwise perceived tilt) or right (for clockwise perceived tilt) arrow key button on a keyboard. The no-adaptation condition was identical to the adaptation condition, except there was no adapter before the test. The experiment contained a total of 1500 trials (2 experimental conditions [Adaptation and No-adaptation] x 2 adaptive staircases x 25 trials x 15 test locations). Participants were debriefed after the experiment.

We calculated the point of subjective verticality (PSV) (i.e., the angle at which the participant would report the perceived tilt as clockwise 50% of the time) by fitting a logistic regression function using Psignifit 4 MATLAB Toolbox (Schütt, Harmeling, Macke, & Wichmann, 2016). For each participant, 30 PSV values were calculated (2 experimental conditions x 15 test locations) using an equal asymptote method of Psignifit. Next, the TAE magnitude was calculated as

$$\text{TAE magnitude} = PSV_{\text{Adaptation}} - PSV_{\text{No-adaptation.}} \quad (1)$$

A positive TAE magnitude implies a counter-clockwise 'repulsion' away from the adapter orientation; a negative value implies a clockwise 'attraction' towards the adapter orientation.

Statistical analyses were performed on the calculated TAE magnitudes using the JASP software (JASP Team, 2020). First, to answer our research question, we performed a pre-planned two-tailed one-sample t-test to test whether the TAE magnitude is significantly different from zero at each test location (TAE magnitude $\neq$ 0) using the pooled data from both visual hemifields. FDR correction was performed to correct for multiple comparisons. Additionally, we performed a mixed ANOVA with posthoc pairwise t-tests to test the effects of the row, column, and visual hemifield (i.e., within- and between-subject factors) on the TAE magnitude. Finally, to characterize the spread of TAE, we created a map of TAE magnitudes across the visual hemifield and fitted a 2D Gaussian function to it. We used natural neighbor interpolation to predict TAE magnitudes between test positions.

2.2. Results

Fig. 4 top panel shows the observed TAE magnitudes for all test locations as a map. Because the TAE magnitudes did not systematically vary between the hemifields, the results are averaged and represented on the right visual hemifield (no main effect of visual hemifield in between-subject mixed ANOVA, $F(1,17) = 2.16, p = 0.16$). This map clearly shows that TAE is not limited to the adapter location, and it spreads across the visual hemifield. The pre-planned one sample t-tests revealed that this spread of TAE was significant at all test locations (FDR corrected $ps < 0.05$) except D_{N2} (FDR corrected $p = 0.17$).

Furthermore, the spread of TAE depended on the location of the test patch. Specifically, within-subject effects of the mixed ANOVA revealed a significant interaction of the test rows and columns (Sphericity was corrected by Greenhouse-Geisser correction $F(4,61) = 41.33, p = 0.01$), as shown in Fig. 5. As can be observed with a visual inspection of the figure, the TAE magnitude was significantly higher at the center row where the adapter and fixation point were located compared to other rows (FDR corrected $ps < 0.005$) for all test columns except *N2* and *F2*. Pairwise comparisons of the test columns showed significantly higher TAE magnitude at the Center column where the adapter was located compared to all other columns (FDR corrected $ps \leqslant 0.004$). The TAE magnitude decreased with the distance between the test and the adapter. This decrease was proportional to the absolute value of the distance and did not depend on the direction (no significant difference between *N2* and *F2* columns (FDR corrected $p = 0.1$), and between *N1* and *F1* columns (FDR corrected $p = 0.1$), and between Up and Down rows (FDR corrected $p = 0.33$)). Overall, a 2D Gaussian centered at the adapter location ($\sigma_x = 5.02, \sigma_y = 2.93$) could well characterize the spread of TAE.

3. Computational model

Next, in order to establish a link between the behavioral results and

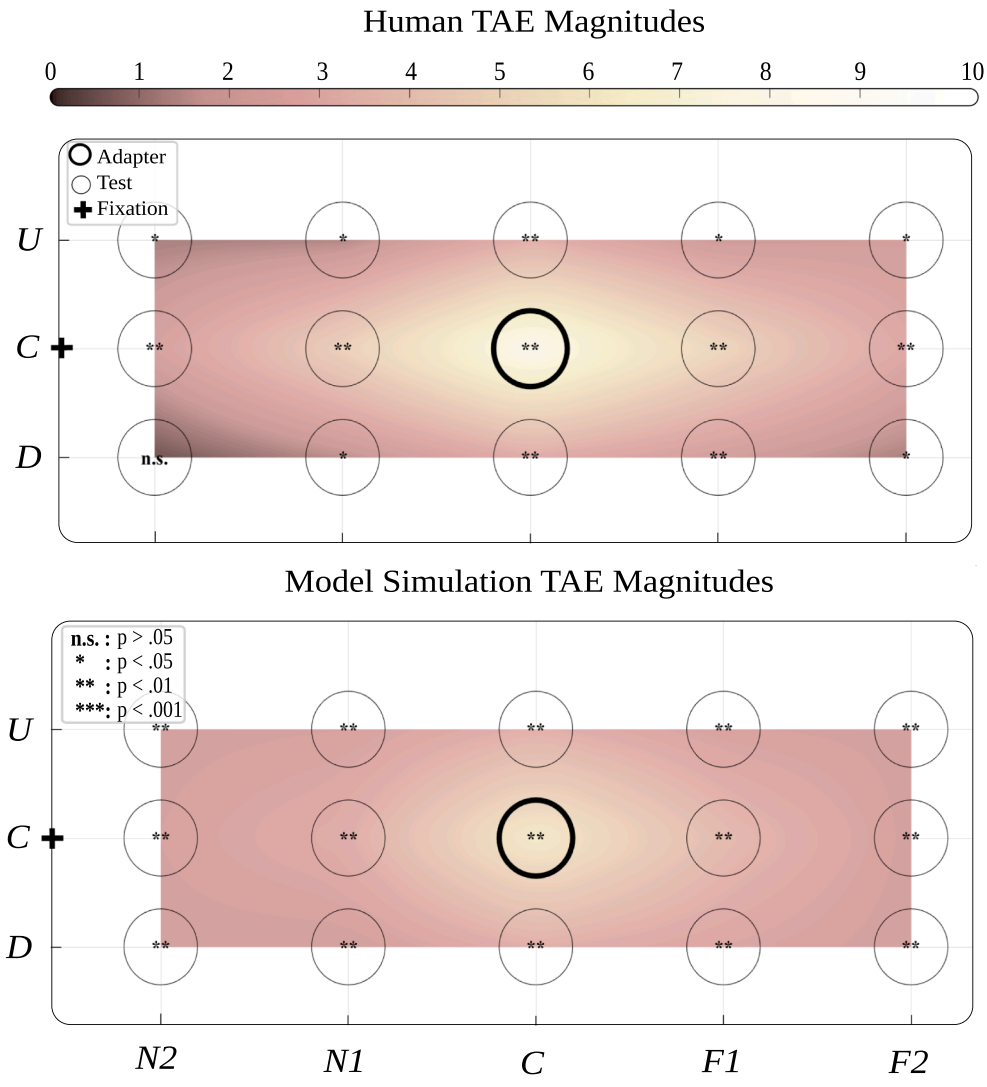

Fig. 4. The TAE magnitudes calculated for the human behavioral experiment (top panel) and model simulation (bottom panel) are shown as a map. The TAE magnitudes for the positions between the test positions were calculated by natural neighbor interpolation. As shown in the top color bar, brighter colors indicate higher TAE magnitudes. The cross sign shows the fixation point location, and circles represent the test positions (see Fig. 2 for naming convention). The bold circle located at the center row and center column (C_c) indicates the location where the adapter patch was presented. Both maps demonstrate that TAE is a non-local aftereffect and spreads across the visual hemifield. Star signs: FDR corrected significance levels.

possible underlying neuronal mechanisms, we have developed and tested a biologically plausible toy model (publicly available, see Data and Code Availability Statement section). The model had an encoding and a decoding component (layer) and its schematic representation is shown in Fig. 6. The encoding component was composed of populations of orientation-tuned units on a grid covering the visual hemifield.

The decoder component estimated the orientation and tilt based on the input it received from the encoding component. While calculating the responses of the orientation-tuned units in the encoding component, we used both shift and suppression mechanisms of adaptation (Jin et al., 2005; Alink et al., 2018). Accordingly, our model assumed that, after adaptation, unit responses could decrease (suppression), and their preference could shift away from the adapter orientation as shown in Fig. 1. To fit the model to the observer data, we optimized the shift and suppression parameters, as well as the RF sizes using a machine learning procedure. We were particularly interested in the optimized RF sizes since they could potentially inform us about possible cortical origins of the spread of TAE.

3.1. Model architecture & optimization

Encoding: We simulated the encoder unit responses on a 20 x 20 visual grid across a hemifield, where lattice points were separated by 1° of visual angle. At each lattice point, we positioned a population of orientation-tuned units ($N = 180$) modeled using a Gaussian-shaped function where the maximum response was equal to 1, and half-width at half-height was equal to 30° (Westrick, Heeger, & Landy, 2016). The preferred orientations of these units were spaced by a 1° polar angle. Inspired by the term 'hyper-column' in the primary visual cortex (V1), we will refer to these multi-unit structures at each lattice point as *hyper-units*.

The response of an encoder unit with receptive field center x,y, and preferred orientation ψ is computed as a weighted product of its tuning curve and RF profile:

$$A_{\psi,x,y}(\theta_s, x_s, y_s) = w_\psi \exp\left(-\frac{(\theta_s - (d_\psi . b_\psi + \psi))^2}{2\sigma_f^2}\right) \exp\left(-\frac{1}{2}\left(\frac{(x-x_s)^2}{\sigma_x^2} + \frac{(y-y_s)^2}{\sigma_y^2}\right)\right), \quad (2)$$

where x_s,y_s and θ_s are the stimulus position and orientation, σ_f is the width of the tuning curve, σ_x and σ_y are the size parameters for the two dimensional RF profile, and w_ψ and b_ψ are the parameters defining the

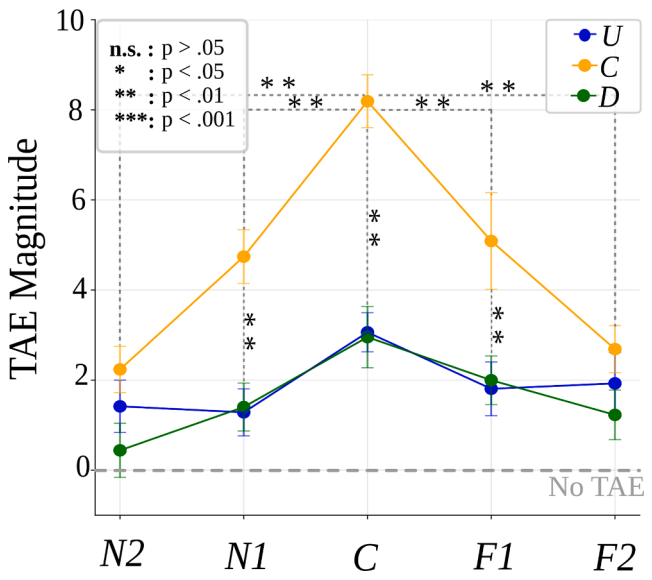

Fig. 5. Human TAE magnitudes are re-plotted. The x-axis represents the test columns, and color-coded lines represent the test rows (the naming convention is the same as in Fig. 2). The within-subject effects of the mixed ANOVA revealed a significant interaction of test rows and columns, showing that the spread of TAE depends on the location of the test grating. Star signs: FDR corrected significance levels. Error bars: standard error of the mean.

amount of suppression and shift of the tuning curve of that unit after adaptation, respectively (we have dropped the indices x, y for clarity). The direction of the tuning curve shift was determined by $d_\psi = \mathrm{sgn}(\psi - \theta_a)$ to ensure that the shift was always away from the adapter orientation, θ_a (sgn(), sign function).

To model the suppression and shift, we first computed the unit responses during the adapter period using Eq. 2 with $w_\psi = 1, b_\psi = 0$, and stimulus variables θ_a, x_a, y_a. We assumed that the adaptation of a unit is related to its activation during the adapter period and modeled this relation using power functions:

$$\begin{aligned} w_\psi &= 1 - \alpha_1 (A_{\psi,x,y}(\theta_a, x_a, y_a))^{\alpha_2}, \\ b_\psi &= \beta_1 (A_{\psi,x,y}(\theta_a, x_a, y_a))^{\beta_2}, \end{aligned} \tag{3}$$

with the constrains $w_\psi \in [0, 1]$ and $b_\psi \geqslant 0$, and α_i and β_i are optimized free parameters. We also assumed $w_\psi = 1$ and $b_\psi = 0$ during the no-adaptation trials.

Decoding: Based on the responses from the encoder layer, the decoder estimated the orientation of the input stimulus θ_s ($\hat{\theta}_s$) for stimulus location (x_s, y_s) using the winner-take-all method with a suitable differentiable approximation to the argmax function

$$\hat{\theta}_s = \underset{\psi}{\mathrm{argmax}}(A_{\psi,x_s,y_s}) \approx \sum_{\psi}^{180} \left(\frac{\gamma A_{\psi,x_s,y_s}}{\sum_j \gamma A_{j,x_s,y_s}} \cdot \psi \right). \tag{4}$$

Next, the decoder returned a probability that the input stimulus is tilted clockwise as

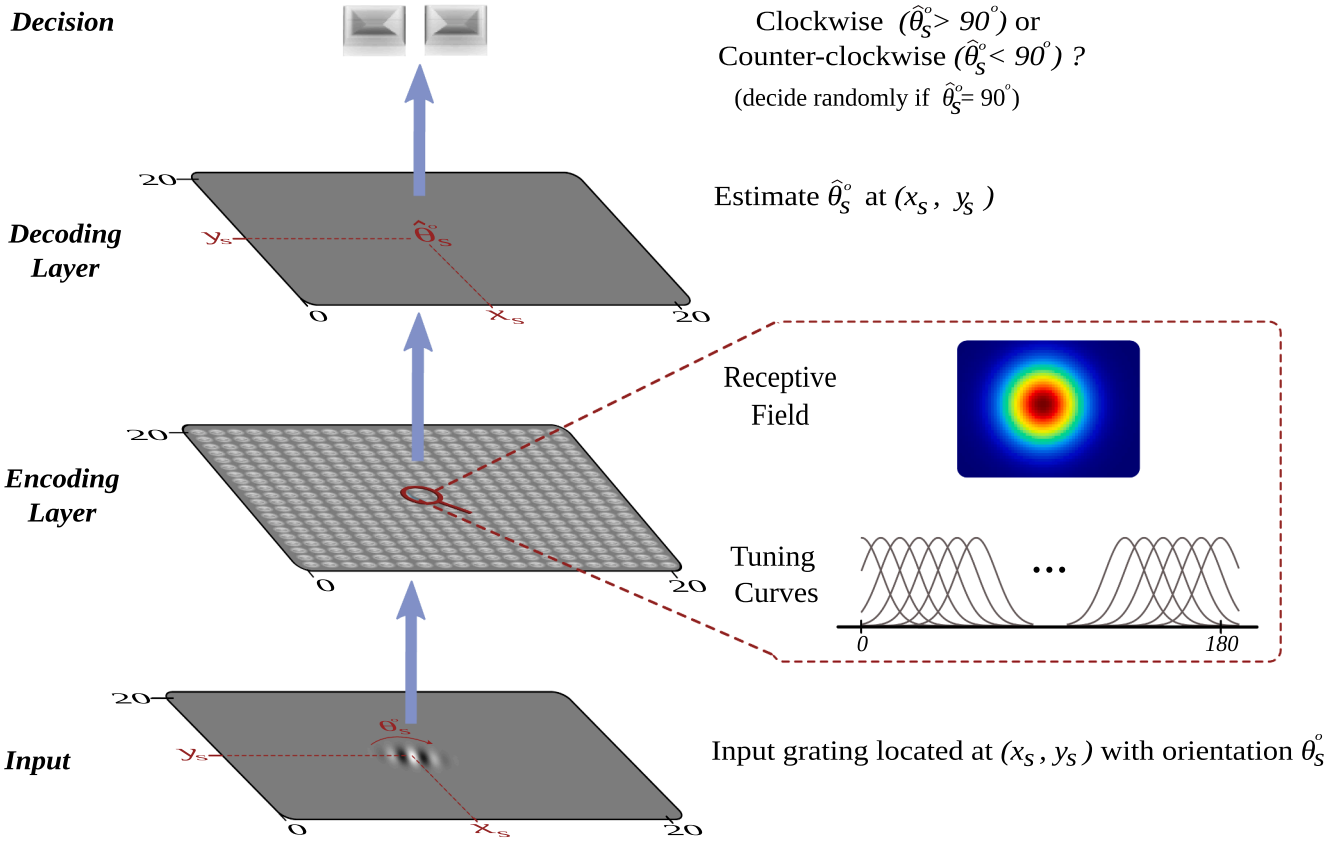

Fig. 6. Schematic representation of the model architecture. The model takes grating located at (x_s, y_s) with orientation θ_s^o as input and encodes the perceived orientation at the given location through the encoding units. Then, based on the response of the encoder, the decoder estimates the orientation of the input stimulus ($\hat{\theta}_s$). Based on the estimation of the decoder, our model outputs a decision for the perceived tilt of the input stimulus that is clockwise if $\hat{\theta}_s > 90°$ and counter-clockwise if $\hat{\theta}_s < 90°$. If $\hat{\theta}_s = 90°$, the model makes a random decision.

Table 1
Variables and optimized parameters used in the computational model.

Symbol	Description	
θ_a, x_a, y_a	orientation & position of the adapter grating	
θ_s, x_s, y_s	orientation & position of the test grating	
ψ, x, y	preferred orientation & RF center of a simulated encoder unit	
σ_f	width of the orientation tuning curve of an encoder unit	
σ_x, σ_y	two-dimensional RF size parameters of an encoder unit	optimized
$A_{\psi,x,y}(\theta_s, x_s, y_s)$	activation of an encoder unit	
d_ψ, b_ψ	direction, and magnitude of tuning curve shift of the encoder unit with preferred orientation ψ	
w_ψ	suppression parameter of an encoder unit with preferred orientation ψ	
β_1, β_2	parameters of the power function governing b_ψ	optimized
α_1, α_2	parameters of the power function governing w_ψ	optimized
$\widehat{\theta}_s$	predicted orientation of the test grating by the decoder	
$\widehat{\rho}_s$	probability that test grating is tilted clockwise as reported by the decoder	

$$\widehat{\rho}_s = \max\left(0, \min\left(1, \frac{\widehat{\theta}_s - 89}{2}\right)\right), \tag{5}$$

where $\widehat{\rho}_s = 0.5$ when the predicted stimulus orientation is vertical ($\widehat{\theta}_s = 90$). Table 1 summarizes all the variables and optimized parameters in our model.

We implemented and optimized the model using the PyTorch library in Python (Paszke et al., 2019). The training was done on randomly selected 80% of the adaptation condition data. Testing the model performance was done on the remaining 20% of the adaptation condition data, as well as on randomly selected 20% of the no-adaptation condition data. We trained the model separately for each participant and optimized b_ψ, w_ψ, σ_x, and σ_y parameters. Optimization was performed using the adaptive moment estimation (Adam) optimization (Kingma & Ba, 2014). The model architecture was the same for adaptation and no-adaptation conditions, but because no suppression and shift are expected on the no-adaptation condition, we set $b_\psi = 0$ and $w_\psi = 1$ and used the σ_x and σ_y parameters optimized for the adaptation condition. Therefore, we did not perform training for the no-adaptation condition, and this simulation served as a control for our model's performance.

3.1.1. Model performance & simulations

To measure the model's performance, we tested the model on the test sets for both adaptation and no-adaptation conditions. We calculated the accuracy as the percentage of correctly predicted tilt directions and used this as a metric of model performance evaluation.

Table 2
Optimized parameters of the power functions determining suppression and shift (w_ψ and b_ψ, see Eq. 3) along with their standard error of the mean values in parentheses. Values were averaged across participants.

α_1	α_2	β_1	β_2
0.67 (0.05)	0.29 (0.04)	0.74 (0.07)	0.17 (0.04)

Next, using the optimized parameters per participant, we made our model run the same behavioral experiment for adaptation and no-adaptation conditions. Based on the simulated responses, we first obtained the TAE magnitudes via the same method used in the behavioral experiment. Then, we performed a two-tailed one-sample t-test to test whether TAE magnitudes are significantly different from zero at each location (multiple comparisons were corrected by FDR correction) and formed the same TAE magnitude map as in the behavioral experiment. Finally, to compare the TAE magnitudes in human and simulated data, we calculated a cosine similarity score between them. To test whether the score is statistically significantly different than the chance level, we generated a null distribution of 1000 cosine similarities based on randomly shuffled data and computed an achieved significance level.

3.2. Model results

The model could predict the human behavioral data above the chance level (50%) for adaptation and no-adaptation conditions at all test locations (Fig. 7). The average accuracy for the adaptation condition was 76.9% ($SD = 0.13$), and the average accuracy for the no-adaptation condition was 66.7% ($SD = 0.19$). Furthermore, an inspection of the model simulation and human TAE magnitude maps in Fig. 4 reveals a closely matching pattern (cosine similarity $= 0.70$, achieved significance < 0.01). These results show that the model matches human data closely.

Next, to validate that the model behaves reasonably, we evaluated the optimized suppression and shift values. Table 2 reports the optimized parameters of the power functions (Eq. 3), and Fig. 8 shows the suppression and shift values derived from those parameters. Consistent with the behavioral results, and as expected based on the findings in the literature, the model predicted stronger suppression and larger shift for units whose RF centers are closer to the adapter position and whose preferred orientations are closer to the adapter orientation. Suppression and shift decreased as the distance between the unit RF center and the adapter position increased and as the difference between the preferred orientation of the unit and the adapter's orientation increased. These results show that the internal workings of the model are consistent with the behavioral results and findings in the literature.

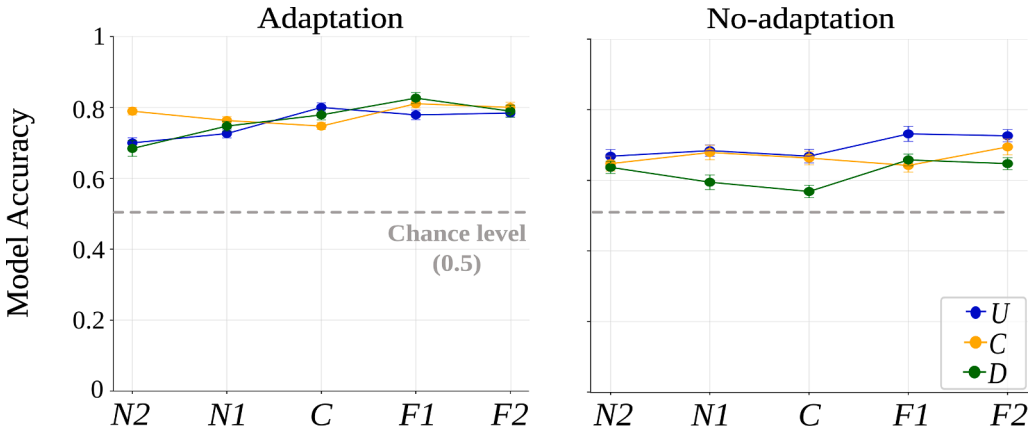

Fig. 7. Model accuracy for adaptation (left panel) and no-adaptation (right panel) conditions. The x-axis and color-coded lines represent test columns and rows, respectively (the naming convention is the same as in Fig. 2). First, we fit the model to each participant's data. Then, we used the trained model to predict unseen data of the participant and calculated the accuracy. Finally, we averaged the obtained accuracy values across participants. Error bars: standard error of the mean.

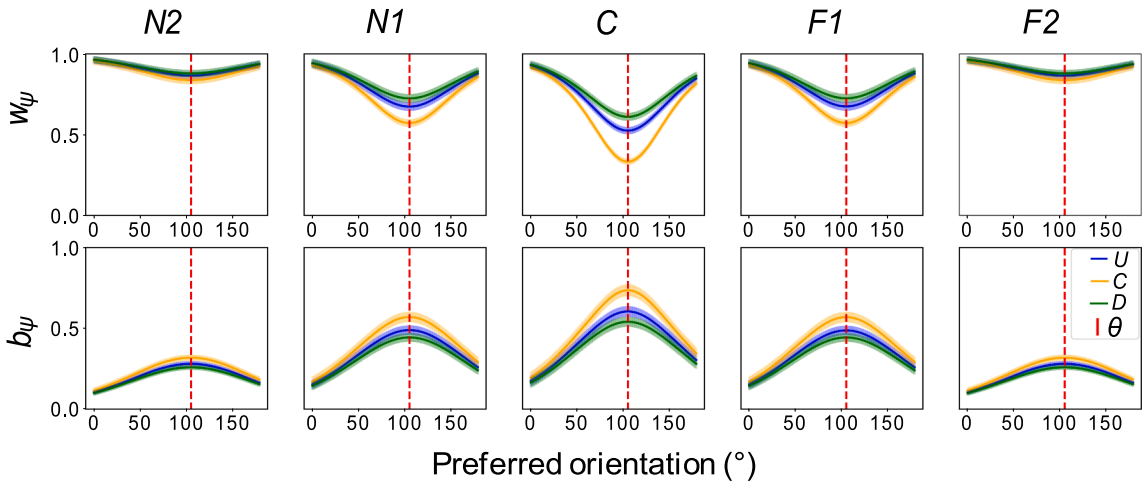

Fig. 8. Suppression, w_ψ, and shift, b_ψ, values predicted by the model. Smaller w_ψ values mean stronger suppression, and larger b_ψ mean larger shift. Panels and color-coded solid lines indicate the RF center positions, and the x-axes indicate the preferred orientations of the encoder units (panels: horizontal positions; color-coded lines: vertical positions). The dashed vertical red lines mark the adapter orientation (θ_a). The transparent thickness of the solid lines represents the standard error of the mean. Stronger suppression and shift are observed at units with RF centers and preferred orientations closer to the adapter position and orientation.

Table 3
Optimized values of two-dimensional RF size parameters, σ_x,σ_y, along with their SEMs in parentheses. Same as in Table 2, the values were obtained by averaging the optimized RF size parameters across participants.

	N2	*N1*	*C*	*F1*	*F2*
U	3,3	3.3,3.3	3.15,3	3.12,3.12	3,3
	(0.01,0.03)	(0.06,0.06)	(0.04,0.03)	(0.12,0.12)	(0.1,0.1)
C	3.01,3.01	2.95,2.95	3.01,3	3.05,3.05	3,3
	(0.05,0.05)	(0.06,0.06)	(0.04,0.04)	(0.12,0.12)	(0.05,0.03)
D	3,3	3.18,3.18	3.25,3	3.27,3.27	3.05,3.05
	(0.12,0.1)	(0.13,0.13)	(0.11,0.1)	(0.11,0.11)	(0.13,0.1)

Finally, we evaluated the RF size parameters σ_x and σ_y. Table 3 reports their optimized values. This analysis was particularly important because optimized RF size parameters can potentially provide clues about the cortical origins of the behavioral effect. Overall σ_x and σ_y values were around 3 degrees (mean σ_x : 3.09, $SD = 0.12$; mean σ_y : 3.06,$SD = 0.11$). Within each hyper-unit, σ_x and σ_y values did not differ much from each other, which means that the RFs were approximately isotropic. Further, there was no substantial difference between the optimized values for different test locations, which suggests that the modeled RF sizes did not vary with eccentricity (no main effect of location on RF size parameters, Kruskal–Wallis test, $p > 0.05$). We discuss the possible implications of these findings in the next section.

4. Discussion

Here, we studied whether and how the tilt aftereffect (TAE) spreads across the visual field. In our behavioral experiment, we measured the TAE magnitude at fifteen locations within a visual hemifield, including the adapter location. Consistent with the previous literature, our behavioral results showed that a prolonged view of an oriented Gabor patch (adapter) led to changes in the perceived orientation of the subsequently presented test patch at the location of the adapter. Specifically, the perceived orientation of the test patch was repelled away from the orientation of the adapter. But most importantly, our results showed that TAE is not limited to the adapter location; instead, it spreads across the visual hemifield. The spread was systematic: TAE was highest at the adapter location and decreased with the distance between the adapter and the test in a nearly isotropic manner.

Typically, adaptation to low-level visual features is treated as a local effect because responses to low-level features are thought to be localized in the retinotopic space, whereas high-level processes are thought to be more global (e.g., see Bowden, Dickinson, Green, & Badcock (2019)). Our results, however, show that one must be cautious while implying this simple dichotomy and that adaptation to low-level features may also lead to more global effects.

Previous models based on the local TAE results supported the idea that the effect originates in V1 through feedforward mechanisms (e.g. Jin et al., 2005). Could a similar V1 model explain our results here? Or does the spread of the TAE require the involvement of other mechanisms? Conceptually, in a feedforward mechanism, the spread of the effect would require the involvement of neurons with relatively large RFs, which can integrate information across the visual hemifield. To test this, we next developed a feedforward computational model and estimated the RF sizes of hypothetical neurons whose activity could predict the specifics of the spread we observed in our behavioral data.

The computational model could indeed successfully predict the empirical TAE magnitudes at all tested locations in the visual hemifield with high accuracy. Further, the model captured the pattern of the empirical TAE magnitudes. Specifically, it predicted the highest TAE at the location of the adapter, and the simulated TAE magnitudes decreased nearly isotropically as the distance between the adapter and the test increased. As we expected, the optimized RF sizes were relatively large (approximately 3 degrees, on average), and they did not change substantially with eccentricity. Consequently, an ideal candidate visual area whose activity gives rise to the spread of TAE across the hemifield would be the one with relatively large RFs while having selectivity to orientation.

The aforementioned qualities are commonly associated with mid-level visual areas, for example, the visual area V4. V4 is situated along the ventral pathway, and its characteristics include selectivity to orientation and color (Roe et al., 2012; Desimone & Schein, 1987). Its activity is linked to surface perception and completion (Pan et al., 2012; Bouvier, Cardinal, & Engel, 2008), integration of spatial information across the visual space, and perception of illusory contours (De Weerd, Desimone, & Ungerleider, 1996). RF sizes of V4 neurons were found to be 4 to 7 times larger than those of V1 neurons in macaque (Desimone & Schein, 1987). Similarly, a human functional magnetic resonance imaging (fMRI) study found that V4 population receptive fields are larger than those in V1, and importantly, their sizes do not change substantially with eccentricity (van Dijk, de Haas, Moutsiana, & Schwarzkopf, 2016). These RF characteristics are in line with our model predictions. Furthermore, V4 is extensively interconnected with other visual areas. It receives direct inputs from V1 (Nakamura, Gattass, Desimone, &

Ungerleider, 1993), and it is connected to higher-level temporal areas such as TE and TEO, which suggests that it plays a role in object recognition. It is also connected to higher-level dorsal areas such as DP, VIP LIP, PIP, and MST, which suggests that it plays a role in spatial vision and attention, as well (Baizer, Ungerleider, & Desimone, 1991; Ungerleider, Galkin, Desimone, & Gattass, 2008; Kienitz, Kouroupaki, & Schmid, 2022). Thus, we contend that a mid-level visual area, such as V4, appears to be a plausible candidate to be the origin of the spread of TAE across the visual field. However, the exact origin of the effect would require further neuronal investigation.

It should be noted that here we propose a simple feedforward model assuming units with classical receptive fields (cRF). Alternative models incorporating feedback and lateral connections can also be tested. Feedback from higher-level areas could modulate the activity of V1 neurons beyond their cRFs (Angelucci et al., 2017), thus may have a causal relation with the spread of the effect. Likewise, lateral (horizontal) connections within V1, which extend well beyond a neuron's cRF (Stettler, Das, Bennett, & Gilbert, 2002), may have a causal relation with the spread of the effect we found here. In summary, the spread of the aftereffect may also be caused by the activity of neurons with relatively smaller RFs in earlier visual areas that receive feedback and/or lateral projections. Therefore, future studies testing such models in conjunction with neuronal activity in V4 and other visual areas would be required for a better understanding of the origin of the spread of figural aftereffects, including TAE and size aftereffect (Altan & Boyaci, 2020).

Possible role of spatial attention. Encoding the spatial location of a stimulus is argued to be a primary or mandatory process. For example, it was shown that attending to a stimulus feature, with the location being irrelevant, was automatically accompanied by attention to the spatial location that the stimulus occupies (Tsal & Lavie, 1993). Therefore, in our experimental paradigm, adapting to a tilted contour that always appears at the same location within the visual hemifield could automatically trigger spatial attention to that location and enhance the neuronal responses (Gandhi, Heeger, & Boynton, 1999; Treue & Trujillo, 1999). This could play a role in the highest TAE observed at the adapted location. This prediction is consistent with previous studies that demonstrated higher magnitudes of perceptual aftereffects at the attended spatial locations Yeh, Chen, De Valois, and De Valois,. (1996). Even though our model integrates some attentional mechanism by the winner-take-all strategy (Lee, Itti, Koch, & Braun, 1999) to predict the perceived tilt, attention could be explicitly manipulated in future behavioral experiments, and its effects could be more explicitly incorporated into the current model architecture to test these hypotheses further e.g., the normalization model of attention Reynolds and Heeger (2009).

Implications for temporal dynamics of neuronal responses. As discussed above, the activity of visual neurons can be modulated by stimuli presented well beyond their cRF. Feedback and lateral connections within a cortical area are two possible mechanisms that underlie this phenomenon (Angelucci et al., 2017). For example, lateral connections in V1 can be 3 to 8 times the neuron's cRF (Stettler et al., 2002) and may have complex effects on its activity (Sceniak, Ringach, Hawken, & Shapley, 1999; Henry, Jazayeri, Shapley, & Hawken, 2020; Chen, Kasamatsu, Polat, & Norcia, 2001). Our results suggest that these effects may go beyond the spatial domain and include temporal interactions, for which intriguing possibilities exist, such as a delayed normalization model (Groen et al., 2022). Thus, non-local adaptation could be utilized to study the temporal dynamics of feedback and lateral connections, as well as cRF properties.

Potential applications for visual rehabilitation, and implications for perceptual learning. Developing rehabilitation techniques to restore, recover or improve the vision of patients with neural damage is an integral part of vision research. Findings from the literature show that vision could be restored with appropriate perceptual training methods. However, this recovery is often believed to be limited to the trained location and not transferred to other locations in the visual field (for example, in blindsight, Cowey & Stoerig (1991)). Our findings, on the other hand, could encourage work on the development of more efficient training techniques. Specifically, neurons at higher-level visual areas with large RFs could respond to the training stimulus presented at different parts of the visual field. Accordingly, training with a stimulus preferred by neurons in those visual areas could lead to visual improvements that are not specific to the exact location of that stimulus. Indeed, training blindsight patients with a stimulus targeting higher-level visual areas (e.g., a complex optic flow motion stimulus) lead to improvements in untrained locations (Awada, Bakhtiari, Legault, Odier, & Pack, 2022). Further in line with this idea, recent studies in perceptual learning literature provide evidence that learning transfers to other locations with training paradigms that leverage the involvement of higher-level visual areas (Bakhtiari, Awada, & Pack, 2020). These training effects could be explained in part with our findings here.

Implications for computer vision. Recently artificial neural networks (ANNs) have been remarkably successful in computer vision tasks such as object recognition and image segmentation. Yet, these networks do not usually employ temporal and spatial integration together. In particular, sequential training of ANNs through time with a visual feature does not lead to altered perceptions at other locations. Our results here, however, show that such integration processes happen in the human visual system, which could be important for more efficient computational processing of visual information. Therefore, our findings here could have implications for ANNs to achieve more efficient and human-like computer vision systems.

5. Conclusion

To conclude, we have found that prolonged exposure to a tilted Gabor patch affects the perceived orientation of subsequently presented stimuli not only at the adapter's location but also at other parts of the visual field. These results show that adaptation to low-level visual features may not be as local as previously thought. Further, the systematic pattern observed in human data could be predicted by a simple feedforward computational model. Importantly, the optimized RF sizes in the model suggest that the spread of the effect could originate in a mid-level visual area, such as V4. Overall, these results may have implications for temporal and spatial dynamics of neuronal responses, as well as perceptual learning, and they could inform the development of more efficient visual rehabilitation methods and computer vision algorithms.

6. Data and Code Availability Statement

The code for the experimental paradigm and computational model, together with the anonymized data of this study, is publicly available under the GitHub page https://github.com/tugcegurbuz/TAE-spreads-across-the-visual-field.

7. CRediT authorship contribution statement

Busra Tugce Gurbuz: Conceptualization, Data curation, Formal analysis, Investigation, Methodology, Project administration, Software, Visualization, Writing - original draft. **Huseyin Boyaci:** Conceptualization, Supervision, Writing - review & editing.

Declaration of Competing Interest

The authors declare that they have no known competing financial interests or personal relationships that could have appeared to influence the work reported in this paper.

Acknowledgments

This research did not receive any specific grant from funding agencies in the public, commercial, or not-for-profit sectors.

References

Alink, A., Abdulrahman, H., & Henson, R. N. (2018). Forward models demonstrate that repetition suppression is best modelled by local neural scaling. *Nature Communications, 9*, 3854.

Altan, E., & Boyaci, H. (2020). Size aftereffect is non-local. *Vision Research, 176*, 40–47.

Angelucci, A., Bijanzadeh, M., Nurminen, L., Federer, F., Merlin, S., & Bressloff, P. C. (2017). Circuits and Mechanisms for Surround Modulation in Visual Cortex. *Annual Review of Neuroscience, 40*(1), 425–451.

Anstis, S., Verstraten, F. A., & Mather, G. (1998). The motion aftereffect. *Trends in cognitive sciences, 2*(3), 111–117.

Awada, A., Bakhtiari, S., Legault, C., Odier, C., & Pack, C. C. (2022). Training with optic flow stimuli promotes recovery in cortical blindness. *Restorative Neurology and Neuroscience(Preprint)*, 1–16.

Baizer, J. S., Ungerleider, L. G., & Desimone, R. (1991). Organization of visual inputs to the inferior temporal and posterior parietal cortex in macaques. *Journal of Neuroscience, 11*(1), 168–190.

Bakhtiari, S., Awada, A., & Pack, C. C. (2020). Influence of stimulus complexity on the specificity of visual perceptual learning. *Journal of Vision, 20*(6), 13–13.

Blakemore, C., & Campbell, F. W. (1969). On the existence of neurones in the human visual system selectively sensitive to the orientation and size of retinal images. *The Journal of physiology, 203*(1), 237–260.

Blakemore, C., & Sutton, P. (1969). Size adaptation: A new aftereffect. *Science, 166* (3902), 245–247.

Bouvier, S. E., Cardinal, K. S., & Engel, S. A. (2008). Activity in visual area v4 correlates with surface perception. *Journal of vision, 8*(7), 28.

Bowden, V. K., Dickinson, J. E., Green, R. J., & Badcock, D. R. (2019). Phase specific shape aftereffects explained by the tilt aftereffect. *Journal of Experimental Psychology: Human Perception and Performance, 45*(7), 889–910.

Chen, C.-C., Kasamatsu, T., Polat, U., & Norcia, A. M. (2001). Contrast response characteristics of long-range lateral interactions in cat striate cortex. *Neuroreport, 12* (4), 655–661.

Clifford, C. W., Wyatt, A. M., Arnold, D. H., Smith, S. T., & Wenderoth, P. (2001). Orthogonal adaptation improves orientation discrimination. *Vision Research, 41*(2), 151–159.

Cowey, A., & Stoerig, P. (1991). The neurobiology of blindsight. *Trends in neurosciences, 14*(4), 140–145.

Desimone, R., & Schein, S. J. (1987). Visual properties of neurons in area v4 of the macaque: sensitivity to stimulus form. *Journal of neurophysiology, 57*(3), 835–868.

De Weerd, P., Desimone, R., & Ungerleider, L. G. (1996). Cue-dependent deficits in grating orientation discrimination after v4 lesions in macaques. *Visual neuroscience, 13*(3), 529–538.

van Dijk, J. A., de Haas, B., Moutsiana, C., & Schwarzkopf, D. S. (2016). Intersession reliability of population receptive field estimates. *Neuroimage, 143*, 293–303.

Dragoi, V., Sharma, J., & Sur, M. (2000). Adaptation-induced plasticity of orientation tuning in adult visual cortex. *Neuron, 28*(1), 287–298.

Gandhi, S. P., Heeger, D. J., & Boynton, G. M. (1999). Spatial attention affects brain activity in human primary visual cortex. *Proceedings of the National Academy of Sciences, 96*(6), 3314–3319.

Gibson, J. J., & Radner, M. (1937). Adaptation, after-effect and contrast in the perception of tilted lines. I. Quantitative studies. *Journal of Experimental Psychology, 20*(5), 453–467.

Groen, I. I. A., Piantoni, G., Montenegro, S., Flinker, A., Devore, S., Devinsky, O., Doyle, W., Dugan, P., Friedman, D., Ramsey, N. F., Petridou, N., & Winawer, J. (2022). Temporal Dynamics of Neural Responses in Human Visual Cortex. *The Journal of Neuroscience, 42*(40), 7562–7580.

Harris, J., & Calvert, J. (1989). Contrast, spatial frequency and test duration effects on the tilt aftereffect: Implications for underlying mechanisms. *Vision Research, 29*, 129–135.

Henry, C. A., Jazayeri, M., Shapley, R. M., & Hawken, M. J. (2020). Distinct spatiotemporal mechanisms underlie extra-classical receptive field modulation in macaque V1 microcircuits. *eLife, 9*, 1–23.

JASP Team. (2020). JASP (Version 0.13.1)[Computer software].

Jin, D. Z., Dragoi, V., Sur, M., & Seung, H. S. (2005). Tilt Aftereffect and Adaptation-Induced Changes in Orientation Tuning in Visual Cortex. *Journal of Neurophysiology, 94*, 4038–4050.

Kienitz, R., Kouroupaki, K., & Schmid, M. C. (2022). Microstimulation of visual area V4 improves visual stimulus detection. *Cell Reports, 40*(12), 111392.

Kingma, D.P., Ba, J. (2014). Adam: A method for stochastic optimization. arXiv preprint arXiv:1412.6980.

Lee, D. K., Itti, L., Koch, C., & Braun, J. (1999). Attention activates winner-take-all competition among visual filters. *Nature neuroscience, 2*(4), 375–381.

McCollough, C. (1965). Color adaptation of edge-detectors in the human visual system. *Science, 149*(3688), 1115–1116.

McDermott, K. C., Malkoc, G., Mulligan, J. B., & Webster, M. A. (2010). Adaptation and visual salience. *Journal of Vision, 10*(13), 17–17.

Nakamura, H., Gattass, R., Desimone, R., & Ungerleider, L. G. (1993). The modular organization of projections from areas v1 and v2 to areas v4 and teo in macaques. *Journal of Neuroscience, 13*(9), 3681–3691.

Nishida, S., Motoyoshi, I., Andersen, R. A., & Shimojo, S. (2003). Gaze modulation of visual aftereffects. *Vision Research, 43*, 639–649.

Pan, Y., Chen, M., Yin, J., An, X., Zhang, X., Lu, Y., Gong, H., Li, W., & Wang, W. (2012). Equivalent representation of real and illusory contours in macaque v4. *Journal of Neuroscience, 32*(20), 6760–6770.

Paszke, A., Gross, S., Massa, F., Lerer, A., Bradbury, J., Chanan, G., Killeen, T., Lin, Z., Gimelshein, N., Antiga, L., Desmaison, A., Kopf, A., Yang, E., DeVito, Z., Raison, M., Tejani, A., Chilamkurthy, S., Steiner, B., Fang, L., Bai, J., Chintala, S. (2019). Pytorch: An imperative style, high-performance deep learning library. In H. Wallach, H. Larochelle, A. Beygelzimer, F. d' Alché-Buc, E. Fox, R. Garnett (Eds.), Advances in neural information processing systems 32 (pp. 8024–8035). Curran Associates, Inc.

Peirce, J. W., Gray, J. R., Simpson, S., MacAskill, M. R., Höchenberger, R., Sogo, H., Kastman, E., & Lindeløv, J. (2019). Psychopy2: experiments in behavior made easy. *Behavior Research Methods, 51*, 195–203.

Reynolds, J. H., & Heeger, D. J. (2009). The normalization model of attention. *Neuron, 61* (2), 168–185.

Roe, A. W., Chelazzi, L., Connor, C. E., Conway, B. R., Fujita, I., Gallant, J. L., Lu, H., & Vanduffel, W. (2012). Toward a unified theory of visual area v4. *Neuron, 74*(1), 12–29.

Sceniak, M. P., Ringach, D. L., Hawken, M. J., & Shapley, R. (1999). Contrast's effect on spatial summation by macaque V1 neurons. *Nature Neuroscience, 2*(8), 733–739.

Schütt, H. H., Harmeling, S., Macke, J. H., & Wichmann, F. A. (2016). *Vision Research, 122*, 105–123.

Stettler, D. D., Das, A., Bennett, J., & Gilbert, C. D. (2002). Lateral Connectivity and Contextual Interactions in Macaque Primary Visual Cortex. *Neuron, 36*(4), 739–750.

Treue, S., & Trujillo, J. C. M. (1999). Feature-based attention influences motion processing gain in macaque visual cortex. *Nature, 399*(6736), 575–579.

Tsal, Y., & Lavie, N. (1993). Location dominance in attending to color and shape. *Journal of Experimental Psychology: Human Perception and Performance, 19*(1), 131.

Ungerleider, L. G., Galkin, T. W., Desimone, R., & Gattass, R. (2008). Cortical connections of area v4 in the macaque. *Cerebral Cortex, 18*(3), 477–499.

Westrick, Z. M., Heeger, D. J., & Landy, M. S. (2016). Pattern adaptation and normalization reweighting. *Journal of Neuroscience, 36*(38), 9805–9816.

Yeh, S.-L., Chen, I., De Valois, K. K., De Valois, R. L., et al. (1996). Figural aftereffects and spatial attention. *Journal of Experimental Psychology: Human Perception and Performance, 22*(2), 446.